

Geometric tracking control of thrust vectoring UAVs

Davide Invernizzi^a, Marco Lovera^a,

^a*Politecnico di Milano, Department of Aerospace Science and Technology, Via La Masa 34, 20156, Milano*

Abstract

In this paper a geometric approach to the trajectory tracking control of Unmanned Aerial Vehicles with thrust vectoring capabilities is proposed. The control design is suitable for aerial systems that allow to effectively decouple position and orientation tracking tasks. The control problem is developed within the framework of geometric control theory on the group of rigid displacements $SE(3)$, yielding a control law that is independent of any parametrization of the configuration space. The proposed design works seamlessly when the thrust vectoring capability is limited, by prioritizing position over orientation tracking. A characterization of the region of attraction and of the convergence properties is explicitly derived. Finally, a numerical example is presented to test the proposed control law. The generality of the control scheme can be exploited for a broad class of aerial vehicles.

Key words: Geometric control; UAVs, thrust-vectoring.

1 Introduction

The development of Unmanned Aerial Vehicles (UAVs) with thrust vectoring capabilities has grown significantly in recent years. These aerial vehicles are endowed with a propulsion system that can deliver both a net torque and a force with respect to the aircraft frame, which makes them end-effector-like devices. Among the different technological solutions, non-coplanar multi-rotor configurations have shown great potentiality in terms of fast disturbance rejection and maneuverability [10,4,8,20,19,15,18]. Indeed, while the standard coplanar architecture combines good performance and a simple mechanical design, it is inherently under-actuated as it cannot match at the same time position and orientation tracking requirements [6], as the control force can be applied only in the vertical direction of the aircraft frame. As a result, the attitude dynamics is strongly coupled with the translational motion, which forbids arbitrary rotational maneuvering while keeping position. By modifying the direction of the delivered force in the body frame, thrust vectoring vehicles overcome this intrinsic maneuverability limitation and widen the operational range of the under-actuated system. Among the different architectures that have been developed, it is worth to mention the tiltrotor configuration, both with fixed tilted propellers and with an actuation mechanism that allows to tilt the propellers. The lat-

ter approach has been applied to the tricopter [11], in which three propellers can tilt independently around a fixed axis through servo-actuators. A similar but redundant configuration with four tiltable propellers has been proposed and experimentally validated in [20] and more recently in [16] and in [18]. A fully actuated hexacopter with fixed tilted rotors has been developed in [12]. While mechanically simpler, this configuration is less efficient than the tiltable architecture in terms of power consumption, as a larger amount of thrust is required to stay in hover. With respect to this issue, an hexarotor with tilted propellers has been studied in [19], with the aim of optimizing the orientation of the propellers in order to limit the wasted power.

The trajectory tracking control problem for these vehicles is set on the group of rigid displacement $SE(3)$ and is challenging for two main reasons: the maneuver may involve large rotational motions and there may be limitations in the thrust vectoring actuation. When referring to the first issue, the use of minimal parametrizations, *e.g.*, Euler angles, is not suitable, since a single chart cannot cover the whole configuration space, whereas the use of quaternions requires special care, as they doubly cover the special orthogonal group $SO(3)$ and have an intrinsic ambiguity in representing the attitude ([1]). For what concerns the thrust vectoring limitation, the propulsion systems cannot usually deliver the thrust force in any direction of the aircraft frame, thus reducing the actual maneuverability. These issues have been addressed explicitly in [7], where the class of laterally

Email addresses: davide.invernizzi@polimi.it (Davide Invernizzi), marco.lovera@polimi.it (Marco Lovera).

bounded fully-actuated aerial vehicles is introduced to describe systems that can achieve both orientation and trajectory tracking. The limitation in the thrust vectoring is accounted for by prioritizing position over orientation tracking, *i.e.*, if the desired orientation and the control force computed to achieve the desired position are not compliant, only the closest feasible orientation is tracked. The control law proposed in [7] extends the geometric controller for the standard quadrotor platform of [14] and exploits a saturation function to cope with the lateral bounds. A reference orientation is computed at each time step through a minimization procedure to be as close as possible to the desired orientation. In [8], the same control problem is solved for tilttable propellers aerial vehicles, for which the thrust vectoring limitation is given by imposing that the control force can be applied only inside a conical domain around the vertical body axis. By assuming the translational motion to be decoupled from the rotational dynamics, the angular velocity is used as an intermediate control input to modify the thrust direction.

In this work, the trajectory tracking problem for UAVs with a tiltrotor configuration is addressed by exploiting the geometric control theory framework. This allows to overcome parametrization issues and to account by design for topological obstructions. While the rationale behind the proposed approach is similar to [7], the force control law does not require a saturation function to work with and the reference orientation, compliant with the actuation constraint, is generated by means of a dynamic controller. This allows to explicitly include not only a reference attitude, but also a reference angular velocity and acceleration, which are required to prove the exponential convergence. In particular, when the desired attitude is not compatible with the actuation constraint, the platform follows a modified attitude in order to match the position tracking and be as close as possible to the desired orientation. The region of attraction of the control law is explicitly derived by considering the coupled translational-attitude motion. It is worth to remark that the proposed controller can be applied directly to the co-planar underactuated configuration when the thrust vectoring capability is neglected. Furthermore, it allows to increase the region of attraction of the geometric control law proposed in [14], which is limited to an attitude angle error less 90° when only a positive thrust can be delivered by the propellers. This work extends our preliminary results presented in [9]. We propose a method to modify the desired attitude in order to be compliant with the actuation limitation, which significantly increases the region of attraction of the control law proposed in [9].

The paper is organized as follows. In Section 2 a brief review of Lie groups and in particular of the group of three-dimensional rigid displacements is presented, mainly to introduce the notation used throughout the manuscript. Then, the model for the control design is derived and

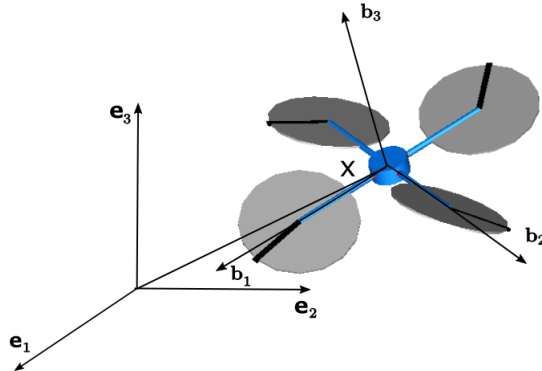


Fig. 1. Reference frame definition

the underlying assumptions are stated. Section 3 introduces the definitions of the configuration errors for the tracking problem. In Section 4, a novel control law for thrust vectoring UAVs which guarantees local exponential convergence on $SE(3)$ is proposed. Section 5 presents the method to compute the reference orientation, which allows to deal with the thrust vectoring limitation; subsequently, in Section 6, a numerical example is reported to check the proposed law.

2 Mathematical modelling

In this section the fundamentals about the group of rigid displacements in the three-dimensional space $SE(3)$ are briefly recalled in order to introduce the notation and ease the reading of the paper. As a first instance, the class of aerial vehicles that are considered in this work can be described as rigid bodies subjected to external actions and with an actuation mechanism that can produce torque in any direction and thrust in a spherical sector region around the vertical axis of the body frame.

2.1 Kinematics

The group of rigid displacements on \mathbb{R}^3 is the set of mappings $g : \mathbb{R}^3 \rightarrow \mathbb{R}^3$ such that $g(p) = x + Ry$, where $R \in SO(3)$ is the rotation matrix which describes the orientation of the body-fixed frame $(O_B, \{b_1, b_2, b_3\})$, $x \in \mathbb{R}^3$ is the position of the origin of B with respect to the inertial frame $(O_I, \{e_1, e_2, e_3\})$ and $y \in \mathbb{R}^3$ is the position of the point p with respect to O_B , resolved in the body frame (see Figure 1).

The motion of the rigid body is an element $G = (R, x) \in SO(3) \times \mathbb{R}^3$. It is often convenient to identify elements of $SO(3) \times \mathbb{R}^3$ with elements in the Special Euclidean Group $SE(3)$ by means of the homogeneous representation

$$(R, x) \mapsto \begin{bmatrix} R & x \\ 0 & 1 \end{bmatrix}. \quad (1)$$

The velocity of a curve $G : [t_0, t_f] \subset \mathbb{R} \rightarrow \text{SE}(3)$ is an element of the tangent space $T_G\text{SE}(3)$ that can be computed as

$$\begin{bmatrix} \dot{R} & \dot{x} \\ 0 & 0 \end{bmatrix} = \begin{bmatrix} R & x \\ 0 & 1 \end{bmatrix} \begin{bmatrix} \hat{\omega} & v_b \\ 0 & 0 \end{bmatrix}, \quad (2)$$

where $\hat{\omega} = R^T \dot{R}$ is the skew-symmetric matrix associated with the body angular velocity and $v_b = R^T \dot{x}$ is the velocity of the body frame origin O_B resolved in the same frame. The tangent space at G is isomorphic to the tangent space at the identity element, *i.e.*, $T_I\text{SE}(3)$, which is the Lie algebra of $\text{SE}(3)$, denoted as $\mathfrak{se}(3)$. In turn, the Lie algebra $\mathfrak{se}(3)$ is isomorphic to $\mathbb{R}^3 \oplus \mathbb{R}^3$ by means of the *hat* map $\hat{\cdot} : \mathbb{R}^3 \oplus \mathbb{R}^3 \rightarrow \mathfrak{se}(3)$:

$$(\omega, v_b)^\wedge = \begin{bmatrix} \hat{\omega} & v_b \\ 0 & 0 \end{bmatrix}. \quad (3)$$

The corresponding inverse isomorphism is the *vee* map $^\vee : \mathfrak{se}(3) \rightarrow \mathbb{R}^3 \oplus \mathbb{R}^3$:

$$\begin{bmatrix} \hat{\omega} & v_b \\ 0 & 0 \end{bmatrix}^\vee = (\omega, v_b) \in \mathbb{R}^3 \oplus \mathbb{R}^3. \quad (4)$$

The same notation $\hat{\cdot} : \mathbb{R}^3 \rightarrow \text{SO}(3)$ is used to define the isomorphism between $\mathfrak{so}(3)$, which is the space of skew-symmetric matrices in $\mathbb{R}^{3 \times 3}$, and \mathbb{R}^3 . The adjoint operator $Ad_G : \mathfrak{se}(3) \rightarrow \mathfrak{se}(3)$ is the derivative of the inner automorphism in $\text{SE}(3)$, $I_G(H) = GHG^{-1}$, along a trajectory passing through the identity in the direction of $\hat{\xi} \in \mathfrak{se}(3)$:

$$Ad_G(\hat{\xi}) = G\hat{\xi}G^{-1}, \quad \hat{\xi} \in \mathfrak{se}(3). \quad (5)$$

In $\text{SO}(3)$ the adjoint operator is used to change the representation from body to inertial

$$\hat{\Omega} = Ad_R \hat{\omega} = R\hat{\omega}R^T \quad (6)$$

or equivalently $\Omega = R\omega$, by exploiting the Lie algebra isomorphism between $\text{SO}(3)$ and \mathbb{R}^3 . The Lie bracket or second adjoint operator $ad_\xi : \mathfrak{se}(3) \rightarrow \mathfrak{se}(3)$ is the derivative of the adjoint operator along a curve passing through the identity element in the direction of $\hat{\eta}$:

$$ad_\xi(\hat{\eta}) = \hat{\xi}\hat{\eta} - \hat{\eta}\hat{\xi} = [\hat{\xi}, \hat{\eta}], \quad \hat{\xi}, \hat{\eta} \in \mathfrak{se}(3). \quad (7)$$

By identifying $\mathfrak{se}(3) \simeq \mathbb{R}^3 \oplus \mathbb{R}^3$ with the hat map isomorphism, the adjoint operator is represented by the linear map

$$ad_\xi = \begin{bmatrix} \hat{\omega} & 0 \\ \hat{v}_b & \hat{\omega} \end{bmatrix}. \quad (8)$$

When referring to $\mathfrak{so}(3) \simeq \mathbb{R}^3$, the adjoint operator is simply

$$ad_\omega = \hat{\omega}. \quad (9)$$

The operator $\langle \alpha, y \rangle$ is the natural pairing of a tangent vector $y \in T_G\text{SE}(3)$ with a covector $\alpha \in T_G^*\text{SE}(3)$. The cotangent space $T_G^*\text{SE}(3)$ is defined as the vector space of linear functionals over $T_G\text{SE}(3)$, denoted as $L(T_G\text{SE}(3), \mathbb{R})$. The differential of a differentiable function $f : \text{SE}(3) \rightarrow \mathbb{R}$ is defined as the covector $df \in T_G^*\text{SE}(3)$ such that

$$\langle df, \dot{G} \rangle = T_G f(\dot{G}) \quad (10)$$

where $T_G f : T_G\text{SE}(3) \rightarrow T\mathbb{R} \simeq \mathbb{R}$ is the restriction at G of the tangent map. By exploiting left translation, the left-trivialized derivative $T_I L_G^*(df)$ is defined as

$$\begin{aligned} \langle df, \dot{G} \rangle &= \langle df, T_I L_G(\hat{\xi}) \rangle \\ &= \langle T_I L_G^*(df), \hat{\xi} \rangle \end{aligned} \quad (11)$$

where $T_I L_G^* : T_G^*\text{SE}(3) \rightarrow \mathfrak{se}^*(3) \simeq (\mathbb{R}^3)^* \oplus (\mathbb{R}^3)^*$ is the cotangent map. When referring to \mathbb{R}^3 and its dual $(\mathbb{R}^3)^*$, the dual basis of the standard basis in \mathbb{R}^3 , $\{e_1, e_2, e_3\}$, is given by $\langle e^i, e_j \rangle = e_i^T e_j = \delta_j^i$, where δ_j^i is the Kronecker delta. Thanks to this identification, $e^i \simeq e_i^T$ and in the following, forces and moments, while actually being covectors in $\mathfrak{se}^*(3)$, are written as standard vectors in $\mathbb{R}^3 \oplus \mathbb{R}^3$.

2.2 Dynamics

This Section briefly recalls the equations of motion of a rigid body moving in a constant gravity field and actuated by a control wrench. The limitations in the tilting capabilities of the actuation mechanism are formally defined.

The kinetic energy of the rigid body can be written in terms of the twist $\xi = (\omega, v_b)$ as

$$T(\dot{G}) = T(G\hat{\xi}) = \frac{1}{2}\mathbb{J}(\omega, \omega) + \frac{1}{2}\mathbb{M}(v_b, v_b) \quad (12)$$

where \mathbb{J} and \mathbb{M} are inner products on \mathbb{R}^3 . The kinetic energy of the rigid body induces an inner product $\mathbb{I} : \mathfrak{se}(3) \times \mathfrak{se}(3) \rightarrow \mathbb{R}$ on the Lie algebra $\mathfrak{se}(3) \simeq \mathbb{R}^3 \oplus \mathbb{R}^3$ by means of

$$\mathbb{I}(\xi, \xi) = \mathbb{J}(\omega, \omega) + \mathbb{M}(v_b, v_b) \quad (13)$$

which in turn defines a left invariant Riemann metric $\mathbb{G}_\mathbb{I} : T\text{SE}(3) \times T\text{SE}(3) \rightarrow \mathbb{R}$ by left translation $\xi =$

$(G^{-1}\dot{G})^\vee$:

$$\mathbb{G}_1(G)(\dot{G}, \dot{G}) = \mathbb{I}\left(\left(G^{-1}\dot{G}\right)^\vee, \left(G^{-1}\dot{G}\right)^\vee\right). \quad (14)$$

Furthermore, it is possible to write (14) as

$$\mathbb{I}\left(\left(G^{-1}\dot{G}\right)^\vee, \left(G^{-1}\dot{G}\right)^\vee\right) = \langle \mathbb{I}^\flat(\hat{\xi}), \hat{\xi} \rangle \quad (15)$$

where $\mathbb{I}^\flat : \mathfrak{se}(3) \rightarrow \mathfrak{se}^*(3)$ is the inertia tensor. By introducing the standard basis for $\mathbb{R}^3 \oplus \mathbb{R}^3$, the action of the inertia tensor (15) on the twist can be written in matrix form as

$$\mathbb{I}^\flat(\xi) = \begin{bmatrix} I & 0 \\ 0 & m \end{bmatrix} \begin{Bmatrix} \omega \\ v_b \end{Bmatrix} \quad (16)$$

where I and m are the inertia matrix and the mass of the body, respectively. By exploiting left trivialization, the equations of motion are obtained in the Euler-Poincaré form [2]

$$\mathbb{I}^\flat(\xi) - \text{ad}_\xi^* \left(\mathbb{I}^\flat(\xi) \right) = w_c + w_g, \quad (17)$$

which can be written explicitly in the standard basis of $\mathbb{R}^3 \oplus \mathbb{R}^3$ as

$$\begin{aligned} I\dot{\omega} + \omega \times I\omega &= \tau_c \\ m(\dot{v}_b + \omega \times v_b) &= f_c - mgR^T e_3. \end{aligned} \quad (18)$$

If the body frame is at the center of mass, the equations of motion can be reduced to

$$\dot{x} = v \quad (19)$$

$$\dot{R} = R\hat{\omega} \quad (20)$$

$$m\dot{v} = -mge_3 + Rf_c \quad (21)$$

$$I\dot{\omega} = -\omega \times I\omega + \tau_c, \quad (22)$$

where $v = Rv_b \in \mathbb{R}^3$ represents the inertial velocity. In this way, the translational motion evolves in the inertial frame, whereas the rotational motion in the body frame. This choice breaks the $\text{SE}(3)$ group structure, but it allows to obtain a simpler expression of the final controller. When the control wrench (f_c, τ_c) spans the whole cotangent space, the system is fully actuated. In the following, the control torque is assumed to span $\mathfrak{so}^*(3) \simeq \mathbb{R}^3$. However, similar to [8], the control force $f_c \in \mathbb{R}^3$ can span only the spherical sector defined around the third body axis b_3

$$0 < \cos(\theta_M) \leq \frac{f_c^T e_3}{\|f_c\|} = \cos(\theta) \quad (23)$$

$$\|f_c\| \leq f_M \quad \forall t \geq t_0, \quad (24)$$

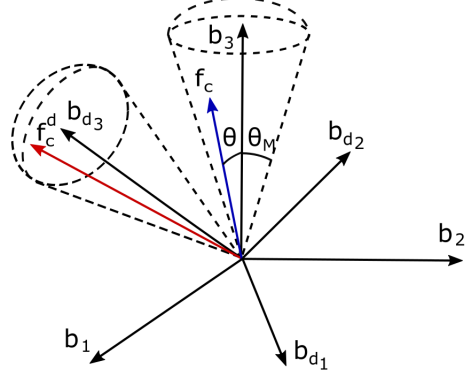


Fig. 2. Spherical sector definition

where f_M is the maximum deliverable control force and the control design becomes more challenging (see Figure 2). This assumption may be a reasonable approximation for UAVs with a tiltrotor configuration, in which the propellers cannot be tilted more than a prescribed angle $\pm\theta_M$ about a fixed axis.

3 Desired trajectory and tracking errors

A smooth tracking command $G_d(t) = (x_d(t), R_d(t)) \in \text{SE}(3)$ is assigned as a function of time and the corresponding velocity command is computed as $\xi_d(t) = (R_d^T v_d, \omega_d)$, where $\omega_d = (R_d^T \dot{R}_d)^\vee$ is the desired body angular velocity and $v_d = \dot{x}_d$ is the desired inertial linear velocity. By assuming the dynamics in (19)-(22), the configuration error for the position and velocity are defined in the inertial frame as

$$e_x = x - x_d \quad (25)$$

$$e_v = v - v_d. \quad (26)$$

For what concerns the attitude dynamics, the left error defined in [2]

$$R_e = RR_d^T \in \text{SO}(3). \quad (27)$$

is employed as the attitude error measure in $\text{SO}(3)$. This choice, uncommon in the literature on UAV control, allows to obtain a simpler expression for the control law. The left attitude error represents the transport map τ_ℓ which is used to compare the desired tangent vector $\dot{R}_d \in T_{R_d}\text{SO}(3)$ in the tangent space of the current orientation $T_R\text{SO}(3)$:

$$\dot{R} - \tau_\ell(\dot{R}_d) = \dot{R} - R_e \dot{R}_d = R(\hat{\omega} - \hat{\omega}_d) \quad (28)$$

from which the left velocity error

$$e_\omega = \omega - \omega_d \quad (29)$$

is defined. The tangent vector $\dot{R}_e \in T_{R_e} \text{SO}(3)$ is computed as

$$\dot{R}_e = \dot{R}R_d^T + R\dot{R}_d^T = R_e \text{Ad}_{R_d} \hat{e}_\omega. \quad (30)$$

For a symmetric positive definite matrix $K_R \in \mathbb{R}^{3 \times 3}$, the well known error navigation function (see, e.g., [5])

$$\Psi = \frac{1}{2} \text{tr}(K_R(I - R_e)) \quad (31)$$

is used in the following analysis. For the sake of simplicity, the gain matrix is assumed to be diagonal

$$K_R = \text{diag}(k_{R_1}, k_{R_2}, k_{R_3}), \quad (32)$$

where $k_{R_1}, k_{R_2}, k_{R_3}$ are strictly positive constants. The main properties of the error navigation function are briefly recalled from [5], adapting the results to the left error representation (27):

- (1) Ψ is locally positive definite about $R_e = I_{3 \times 3}$.
- (2) The left trivialized derivative of Ψ is

$$T_I^* L_{R_e}(d_{R_e} \Psi) = \text{skew}(K_R R_e)^\vee = e_R. \quad (33)$$

- (3) The four critical points of Ψ , for which $e_R = 0$, are $\{R \in \text{SO}(3) : R = R_d \cup R = \exp(\pi \hat{e}_i) R_d\}$.
- (4) For $\Psi < \psi < c_1$ is locally quadratic

$$h_1 \|e_R\|^2 \leq \Psi \leq h_2 \|e_R\|^2 \quad (34)$$

$$h_1 = \frac{c_1}{c_2 + c_3^2}, \quad h_2 = \frac{c_3}{c_1(c_1 - \psi)} \quad (35)$$

where the c_i constants are given by

$$\begin{aligned} c_1 &= \min \{k_{R_1} + k_{R_2}, k_{R_2} + k_{R_3}, k_{R_3} + k_{R_2}\} \\ c_2 &= \max \left\{ (k_{R_1} - k_{R_2})^2, (k_{R_2} - k_{R_3})^2, (k_{R_3} - k_{R_1})^2 \right\} \\ c_3 &= \max \{k_{R_1} + k_{R_2}, k_{R_2} + k_{R_3}, k_{R_3} + k_{R_2}\}. \end{aligned} \quad (36)$$

Based on the above properties and the definition of the left error given in (27), the dynamics of the attitude error vector e_R can be described as in Proposition 1.

Proposition 1 *The time derivative of the attitude error vector e_R is given by*

$$\dot{e}_R = E(K_R, R_e) e_w \quad (37)$$

where $E(K_R, R_e) = \frac{1}{2} (\text{tr}(K_R R_e) I_{3 \times 3} - R_e^T K_R) R_d$.

PROOF. The time derivative of equation (27) reads

$$\dot{e}_R = \frac{d}{dt} \text{skew}(K_R R_e)^\vee = \text{skew}(K_R R_e \text{Ad}_{R_d} \hat{e}_\omega)^\vee \quad (38)$$

$$= \frac{1}{2} (K_R R_e \text{Ad}_{R_d} \hat{e}_\omega + \text{Ad}_{R_d} \hat{e}_\omega R_e^T K_R)^\vee. \quad (39)$$

By exploiting the identity

$$(A^T \hat{x} + \hat{x} A)^\vee = (\text{tr}(A) I_{3 \times 3} - A) x, \quad (40)$$

for $A \in \mathbb{R}^{3 \times 3}$, $x \in \mathbb{R}^3$, the final expression is obtained. The following inequality, useful for the stability analysis, is valid as well

$$\|\dot{e}_R\| \leq \frac{1}{\sqrt{2}} \text{tr}(K_R) \|e_w\|. \quad (41)$$

The proof can be obtained from [5] by considering the left attitude error representation.

4 Control law design

The control force and torque required to track any arbitrary reference for a fully actuated rigid body are:

$$f_c^d = -K_x e_x - K_v e_v + m(\dot{v}_d + g e_3) \quad (42)$$

$$\tau_c = -R_d^T e_R - K_\omega e_\omega + I \dot{\omega}_d + \omega_d \times I \omega. \quad (43)$$

where $K_x, K_v, K_\omega \in \mathbb{R}^{3 \times 3}$ are positive definite gain matrices. The control torque (43), first proposed by [2], has a simpler expression than the one based on the right group error considered in [14] and no cancellation of benign nonlinearities occurs. As in [9], we propose the following modification to the control force to cope with the constraints (23)-(24):

$$f_c = c(\Psi) R_d^T f_c^d, \quad (44)$$

which is the vector with the same components of f_c^d (42) in the desired frame, scaled by a term dependent on the navigation error function Ψ . In particular, the scaling function has to satisfy the conditions:

$$\begin{aligned} \lim_{\Psi \rightarrow 0} c(\Psi) &= 1 \\ 0 < c(\Psi) &\leq 1. \end{aligned} \quad (45)$$

In this work, the scaling function is chosen as $c(\Psi) = \frac{\Psi_M - \Psi}{\Psi_M}$, where $\Psi_M > \psi$. Thanks to this assumption, it is clear that the delivered control force is always within the cone region constraint (23) as long as the desired force f_c^d is kept inside the cone defined around the desired third axis b_{d_3} . Furthermore, it holds true that

$$\|f_c\| = c(\Psi) \|R_d^T f_c^d\| \leq \|f_c^d\|, \quad (46)$$

which means that the constraint (24) is satisfied as long as $\|f_c^d\| \leq f_M$.

Remark 2 *Assume that the attitude error e_R exponentially converges to zero, i.e., $b_i \rightarrow b_{d_i}$; then $R_e \rightarrow I_{3 \times 3}$,*

$c(\Psi) \rightarrow 1$ and the control force $Rf_c = c(\Psi) RR_d^T f_c^d = c(\Psi) R_e f_c^d \rightarrow f_c^d$, which is the control force required to track the desired position.

The formal statement of local exponential convergence is reported in the next Propositions 3, 5.

Proposition 3 (Exponential stability of the attitude motion). Consider the attitude kinematics and dynamics given by equations (20) and (22), the torque control law defined in equation (43) and the closed-loop tracking errors defined in (33), (29). For any positive definite matrices K_ω and $K_R = \text{diag}(k_{R_1}, k_{R_2}, k_{R_3})$, and a constant $\psi < c_1$, where c_1 is given by (36), if the initial conditions satisfy

$$\frac{1}{2} e_\omega^T(0) I e_\omega(0) + \Psi(R_e(0)) < \psi, \quad (47)$$

then, the zero equilibrium of the closed-loop tracking errors $\{e_R, e_\omega\}$ is exponentially stable.

PROOF. The proof is similar to the one in [2] and it is reported in Appendix A.1 for the sake of completeness.

The following definition introduces the concept of feasible reference trajectory, which is essential for the following analysis.

Definition 4 Feasible reference trajectory. A curve $(x_d(t), R_d(t)) \in SE(3)$ is feasible if it is compatible with the spherical sector constraint (23)-(24), i.e., given $b_{d_3} = R_d e_3 \in \mathbb{S}^2$, it satisfies $\forall t \geq t_0$

$$\frac{(f_c^d)^T b_{d_3}}{\|f_c^d\|} \geq \cos(\theta_M) \quad (48)$$

and

$$\|m g e_3 + \dot{v}_d\| \leq f_M^d < f_M \quad (49)$$

where θ_M and f_M are defined in (23)-(24).

It is worth to remark that

$$\cos(\theta_d) = \frac{(f_c^d)^T b_{d_3}}{\|f_c^d\|} = \frac{f_c^T e_3}{\|f_c\|} = \cos(\theta) \quad (50)$$

thanks to the definition of the control force in equation (44). This confirms that the cone region constraint (23) is satisfied as long as the desired attitude motion is feasible, i.e., the angle θ_d between f_c^d and b_{d_3} is less than θ_M . In the following, $\lambda_m(A)$ and $\lambda_M(A)$ represent the minimum and maximum eigenvalue of the real valued matrix A .

Proposition 5 (Exponential stability of the full motion). Consider the translational and rotational dynamics given by equations (19)-(22), the control law defined by (43)-(44), the closed-loop tracking errors defined in (25), (26), (33) and (29) and a feasible reference trajectory (Definition 4). Given $0 < \psi < c_1$, where c_1 is defined by (36), and $0 < f_{c_M} \leq f_M - f_M^d$, where f_M and f_M^d are defined by (24) and (49), respectively, there exist positive definite matrices $K_x, K_v, K_\omega, K_R = \text{diag}(k_{R_1}, k_{R_2}, k_{R_3})$ and a positive constant $\Psi_M > \psi$, such that, if the initial conditions lie in the intersection of the domains

$$\frac{1}{2} e_\omega^T(0) I e_\omega(0) + \Psi(R_e(0)) < \psi \quad (51)$$

and

$$V(0) < \frac{\lambda_m(P_{x1}) f_{c_M}^2}{2 \max(\lambda_M(K_x^T K_x), \lambda_M(K_v^T K_v))}, \quad (52)$$

where V and P_{x1} are given by (A.19) and (A.14), then, the zero equilibrium of the closed-loop tracking error $\{e_x, e_R, e_v, e_\omega\}$ is exponentially stable and the control force is always inside the spherical sector (23)-(24).

PROOF. See Appendix A.2.

The set characterized by (51) and (52) can be widened by increasing c_1 and f_{c_M} . In practice, there are physical limitations due to the actuation mechanism. Indeed, the value of c_1 can be increased with larger rotational gains $k_{R_1}, k_{R_2}, k_{R_3}$, whereas the value of f_{c_M} is limited by the maximum force f_M that can be delivered by the actuation mechanism. Nevertheless, it is also worth to remark that (52) is a conservative condition to keep the control force within the maximum attainable value.

Remark 6 If the tilting capability is "locked", i.e., $\theta_M = 0^\circ$, the platform reduces to the standard underactuated configuration. In this case, the only feasible orientation is represented by the set of rotations around the axis identified by the desired control force. The control force (44) reduces to:

$$f_c = c(\Psi) R_d^T f_c^d = c(\Psi) \|f_c^d\| e_3. \quad (53)$$

As in the solution proposed in [14], i.e.,

$$f_c = \left((Re_3)^T f_c^d \right) e_3 \quad (54)$$

the control force is reduced when the orientation error is large, which is a clear advantage to limit the overshoot in the position tracking. However, equation (54) provides a negative value of the total thrust when the angle between the desired thrust and the vertical body axis is larger

than 90° . On the other hand, according to the proposed law, the total delivered thrust is always positive whenever $\|f_c^d\| \neq 0$, thanks to the definition of $c(\Psi)$, thus being compatible with the requirements of standard VTOL vehicles ($f_c^T e_3 > 0$).

In order to guarantee that the desired control force satisfy the cone region constraint (23), the desired attitude is modified as shown in Section 5.

5 Reference attitude computation

The reference orientation is computed in order to be compliant with the control force that is required to track the desired position. The desired orientation $R_d = [b_{d_1} \ b_{d_2} \ b_{d_3}]$ is assigned as an arbitrary C^2 curve in $SO(3)$. The scheme is built upon the standard geometric approach for underactuated platforms. Since the desired orientation may not be compatible with the position tracking, a reference orientation $R_{dc} \in SO(3)$ is computed in order to be feasible and be as close as possible to the desired attitude. In particular, the reference rotation matrix R_{dc} is decomposed by exploiting the group operation in $SO(3)$ as follows:

$$R_{dc} = R_c R_r \quad (55)$$

where R_r is a relative rotation matrix and R_c is the rotation matrix that is required to track a feasible trajectory in the under-actuated (co-planar) case. More specifically, the base rotation matrix R_c can be selected among the set of rotations around the axis identified by $b_{c_3} = \frac{f_c^d}{\|f_c^d\|}$.

In this work the rotation matrix proposed in [14] was chosen:

$$\begin{aligned} R_c &= [b_{c_1} \ b_{c_2} \ b_{c_3}] \\ b_{c_3} &= \frac{f_c^d}{\|f_c^d\|} \\ b_{c_2} &= \frac{b_{c_3} \times b_{d_1}}{\|b_{c_3} \times b_{d_1}\|} \\ b_{c_1} &= b_{c_2} \times b_{c_3} \end{aligned} \quad (56)$$

in which $b_{d_1} \in \mathbb{S}^2$ is the direction of the first desired body axis. When both the attitude and the position converge to the desired values, the thrust axis b_{c_3} is in the direction of $m(g - \dot{v}_d)$ and the first axis is in the plane spanned by b_{c_3} and b_{d_1} , which is equivalent to assign a desired heading direction.

Remark 7 The definition of the base orientation (56) becomes indeterminate in the degenerate cases when $\|f_c^d\| = 0$ and b_{c_3} is parallel to b_{d_1} . While the former situation can be avoided by employing a nested saturation

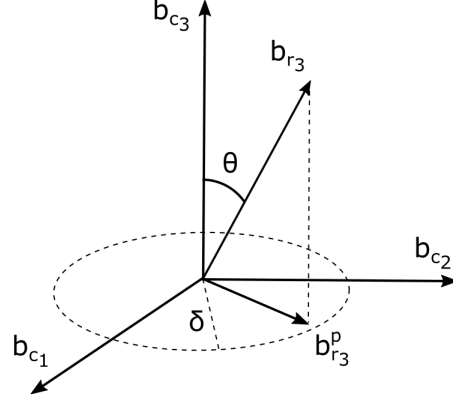


Fig. 3. Reference orientation definition - R_{dc}

approach to define f_c^d (see [17], [8]) or by assuming that

$$\|K_x e_x + K_v e_v\| < \inf_{t \geq t_0} (\|m g e_3 + m \dot{v}_d\|), \quad (57)$$

the latter case can be avoided by selecting a different definition for the axes in the plane orthogonal to b_{c_3} .

The kinematic evolution of the reference trajectory is computed from (55):

$$\dot{R}_{dc} = R_{dc} \hat{\omega}_{dc} \quad (58)$$

$$\omega_{dc} = R_r^T (\omega_c + \omega_r) \quad (59)$$

$$\dot{\omega}_{dc} = -R_r^T \hat{\omega}_r (\omega_c + \omega_r) + R_r^T (\dot{\omega}_c + \dot{\omega}_r). \quad (60)$$

By assuming the angular velocity of the relative trajectory as a control input, it is possible to compute the reference trajectory as the output of a tracking problem in $SO(3)$. In particular, by defining the reference attitude error with a left representation

$$R_e^{dc} = R_{dc} R_d^T \quad (61)$$

and a corresponding Lyapunov candidate

$$\Psi_{dc} = \frac{1}{2} \text{tr} (K_R^{dc} (I - R_e^{dc})) \quad (62)$$

the control input ω_r^d can be obtained by making the derivative of Ψ_{dc} negative definite:

$$\begin{aligned} \dot{\Psi}_{dc} &= \langle T_I^* L_{R_e^{dc}} d\Psi_{dc}, R_d (\omega_{dc} - \omega_d) \rangle \\ &= (R_d^T e_R^{dc})^T (\omega_{dc} - \omega_d) \\ &= (R_d^T e_R^{dc})^T (R_r^T (\omega_c + \omega_r^d) - \omega_d) \end{aligned}$$

$$\omega_r^d = R_r \omega_d - \omega_c - R_r R_d^T e_R^{dc} \rightarrow \dot{\Psi}_{dc} = -\|e_R^{dc}\|^2 \leq 0. \quad (63)$$

In this way, the exponential convergence of the reference trajectory to the desired one is guaranteed. The proof is

similar to the one reported in appendix A.1. Of course, the tracking should be fast enough to follow the desired attitude motion $R_d(t)$ in a reasonable time.

The kinematics of the relative attitude motion $R_r = [b_{r_1} \ b_{r_2} \ b_{r_3}]$ is given by

$$\dot{R}_r = \hat{\omega}_r R_r, \quad (64)$$

where ω_r is modified with respect to ω_r^d in order to be compliant with the cone region constraint. In particular, the differential equation of the third relative axis, $b_{r_3} = R_r e_3$, is modified as follows:

$$\begin{aligned} \dot{b}_{r_3}^p &= \text{Proj} \left(\dot{b}_{r_3}^p, \dot{b}_{r_3}^{pd} \right) \\ \dot{b}_{r_3}^{(3)} &= - \frac{\begin{pmatrix} b_{r_3}^{(1)} \\ b_{r_3}^{(2)} \end{pmatrix}^T \dot{b}_{r_3}^{(1)} + \begin{pmatrix} b_{r_3}^{(2)} \\ b_{r_3}^{(1)} \end{pmatrix}^T \dot{b}_{r_3}^{(2)}}{\sqrt{1 - \left(b_{r_3}^{(1)} \right)^2 - \left(b_{r_3}^{(2)} \right)^2}} \end{aligned} \quad (65)$$

where $b_{r_3}^p = \left\{ b_{r_3}^{(1)}, b_{r_3}^{(2)} \right\}$ is the projection of the vector b_{r_3} in the plane spanned by $\{b_{c_1}, b_{c_2}\}$, $\delta = \sin(\theta_M)$ defines the maximum value of $\|b_{r_3}^p\|$ in order to keep b_{r_3} inside the cone region and $\dot{b}_{r_3}^{pd} = \left\{ \dot{b}_{r_3}^{d(1)}, \dot{b}_{r_3}^{d(2)} \right\}$ is the vector of the first two components of $\dot{b}_{r_3}^d = \omega_r^d \times b_{r_3}$, which is the differential equation describing the relative, desired, third body axis. The projection operator is defined as a function which smoothly removes the radial component of $\dot{b}_{r_3}^p$. In this way, the modulus of $b_{r_3}^p$ is kept within the maximum admissible value according to the cone region constraint. In this work, the weighted projection operator, as defined in [13], is employed:

$$\text{Proj}(\dot{b}_{r_3}^p, \dot{b}_{r_3}^{pd}, f) = \begin{cases} \dot{b}_{r_3}^{pd} - f(b_{r_3}^p) \frac{\Gamma \nabla f(b_{r_3}^p) \nabla f(b_{r_3}^p)^T}{\|\nabla f(b_{r_3}^p)\|_\Gamma^2} \dot{b}_{r_3}^{pd}, \\ \text{if } f(b_{r_3}^p) > 0 \wedge \begin{pmatrix} \dot{b}_{r_3}^{pd} \\ \dot{b}_{r_3}^{pd} \end{pmatrix}^T \nabla f(b_{r_3}^p) > 0 \\ \dot{b}_{r_3}^{pd}, & \text{otherwise} \end{cases} \quad (66)$$

where $f(b_{r_3}^p)$ is a convex continuously differentiable function, and $\nabla(\cdot) : \mathbb{R} \rightarrow \mathbb{R}^2$ is the gradient operator. The function $f(b_{r_3}^p)$ is defined as:

$$f(b_{r_3}^p) = \frac{(1 + \varepsilon) \|b_{r_3}^p\|^2 - \delta^2}{\varepsilon \delta^2} \quad (67)$$

with $\varepsilon \in (0, 1)$, and δ the upper bound on $\|b_{r_3}^p\|$. Since the projection operator, as defined in (66), is continuous but not differentiable, the relative angular acceleration cannot be used in the feedforward term of equation (60). This is a minor issue, as the contribution is usually negligible in practice [8], which is confirmed by the following numerical analysis. Regardless, the smooth version of the projection operator can be employed as defined in [3]. The choice of the positive constant ε is a tradeoff between the realization of the desired orientation tracking

and the effort required by the torque actuation mechanism. It can be proven that (see [13]), when

$$\|b_{r_3}^p\| \in \left[\frac{\delta}{\sqrt{1 + \varepsilon}}, \delta \right], \quad (68)$$

the projection operator starts to operate, enabling a smooth transition towards the bound δ . Hence, the b_{r_3} axis is kept inside the cone defined by the angle θ_M around b_{c_3} and, by referring to equation (50), it is possible to infer that

$$\cos(\theta) \geq \cos(\theta_M) \quad \forall t \geq t_0. \quad (69)$$

As a consequence, if the reference trajectory is inside the cone region at the initial time, it will never leave it. Finally, the angular velocity to drive the relative orientation is defined by:

$$\omega_r = b_{r_3} \times \dot{b}_{r_3} + (b_{r_3}^T \omega_r^d) b_{r_3}. \quad (70)$$

When $\|b_{r_3}^p\| < \frac{\delta}{\sqrt{1 + \varepsilon}}$, $\dot{b}_{r_3} = \omega_r^d \times b_{r_3} = \dot{b}_{r_3}^d$, which in turn implies that $\omega_r = \omega_r^d$. Hence, the desired angular velocity is exactly matched when feasible and, as a consequence, the desired orientation is tracked as well.

6 Numerical results

A simulation example is presented to demonstrate the effectiveness of the proposed controller. The inertial and geometric parameters for the simulation are:

$$I = \text{diag}(0.0074, 0.0074, 0.05) \text{ kg} \cdot \text{m}^2, \quad m = 1.9 \text{ kg} \quad (71)$$

The maximum tilt-angle θ_M is set to 60° , which defines the admissible cone region. The selected controller gains are selected in order to satisfy the assumptions of Proposition 5:

$$\begin{aligned} K_R &= 10 I_{3 \times 3} \text{ kg} \cdot \text{m}^2 \cdot \text{s}^{-2}, \quad K_x = 15 I_{3 \times 3} \text{ kg} \cdot \text{s}^{-2} \\ K_\omega &= I_{3 \times 3} \text{ kg} \cdot \text{m}^2 \cdot \text{s}^{-1}, \quad K_v = 10 I_{3 \times 3} \text{ kg} \cdot \text{s}^{-1} \end{aligned} \quad (72)$$

and $K_R^{dc} = 2K_R$, $\Psi_M = 60 \text{ J}$. Furthermore, $\psi = 12 \text{ J}$, $f_M = 60 \text{ N}$ and the parameters of the projection operator are $\varepsilon = 0.01$ and $\Gamma = 10 I_{2 \times 2}$. A circular trajectory is considered

$$x_d(t) = \left\{ \cos(t), \sin(t), 1 \right\} \text{ m} \quad (73)$$

combined with a superimposed rotation

$$R_d = [-n_d, -b_d, t_d] R_{t_d}, \quad R_{t_d} = \begin{bmatrix} \cos(\theta_d) & -\sin(\theta_d) & 0 \\ \sin(\theta_d) & \cos(\theta_d) & 0 \\ 0 & 0 & 1 \end{bmatrix}, \quad (74)$$

where $t_d = \frac{v_d}{\|v_d\|}$ is the tangent vector to the curve (73), $b_d = \{0, 0, -1\}$, $n_d = b_d \times t_d$ and the superimposed reference angle is $\theta_d(t) = 60^\circ \sin(t)$. The reference curve (solid line) is shown in Figure 4, together with the actual path of the rigid body (dotted line), recovering from $x(0) = \{1.1, 0.1, -0.1\}$ m, $v(0) = \{0, 0, 0\}$ m/s and an attitude error of -100° around the roll axis with null angular velocity, $\omega(0) = \{0, 0, 0\}$ rad/s. Figure 5 confirms the convergence of the position to the desired one. Indeed, the ideal control force is exactly matched after the initial transient phase, as shown in Figure 6, as soon as the attitude error vanishes. Figure 7 shows that the modulus of the control force is always below the maximum allowable value and that the region defined in (52) is conservative. The orientation tracking performance is illustrated in Figure 8. It is worth to underline the large variation in terms of orientation angles, which is naturally handled by the geometric approach. Both the navigation function for the desired R_d and for reference orientation R_{dc} are plotted. As expected, when the desired orientation is not feasible, only the reference orientation R_{dc} is exactly tracked and there is a small error with respect to the desired one. To better understand what happens, Figure 9 shows the absolute value of the angles between the unit vector $-b_d$ (74) and, respectively, the third body axis b_3 and the desired third axis b_{d3} , which are denoted as α and α_d , respectively. When the desired orientation is a clockwise rotation around the roll axis (pointing inside the circle), the desired trajectory is tracked exactly. In the opposite condition, a lower value of the inclination angle is reached because the required control force is always pointing inside the circle and the tracking of the maximum desired angle would imply the violation of the cone region constraint. The value of the cosines between the desired control force f_d and b_{d3} and between the actual control force f_c and b_3 , are shown in Figure 10 to confirm that the control force is always inside the admissible cone region with the prescribed tilt-angle limitation.

7 Conclusions

In this paper, the problem of designing a control law for UAVs with thrust vectoring capabilities has been addressed. The geometric control theory framework has been exploited to develop a control law which guarantees local exponential stability on $SE(3)$ and allows to deal with an approximation of the actuation constraints. Specifically, provided that the reference trajectory is feasible, the total control force is kept within a cone defined by the maximum tilt angle of the propulsive system. The reference orientation is assigned as the output of a controller that tracks an arbitrary desired orientation or the closest attitude whenever the desired orientation is not compatible with the position tracking. Numerical tests have been performed to check the proposed control design. Future works foresee the enhancement of the controller with integral action, which is non-trivial

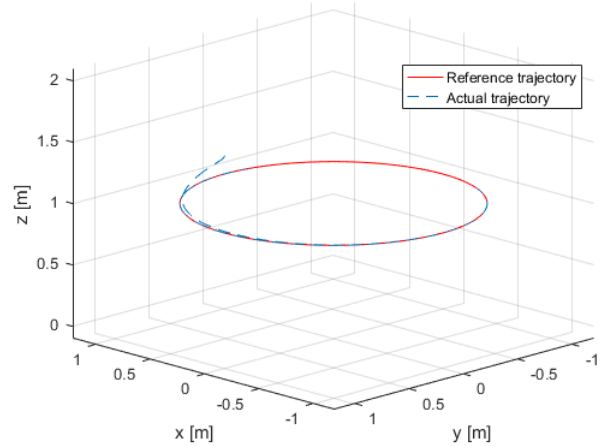


Fig. 4. Reference trajectory

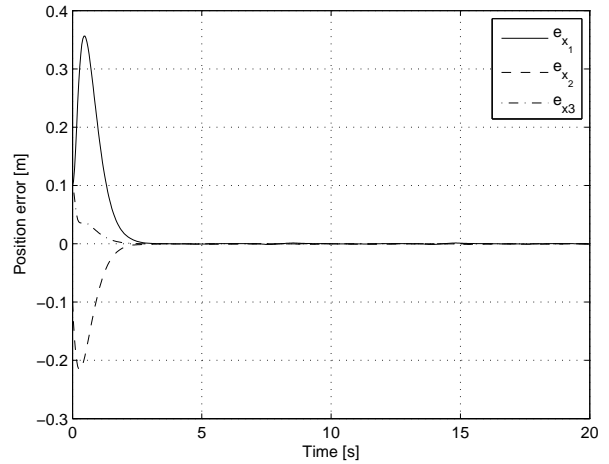


Fig. 5. Position tracking error e_x

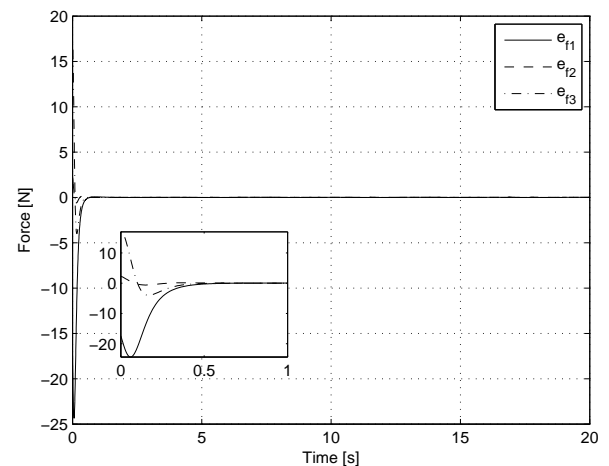


Fig. 6. Control force error - $e_f = f_c^d - Rf_c$

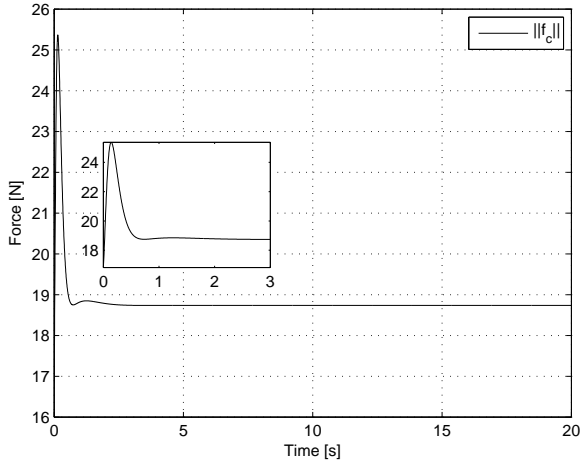


Fig. 7. Modulus of the delivered control force - $\|f_c\|$

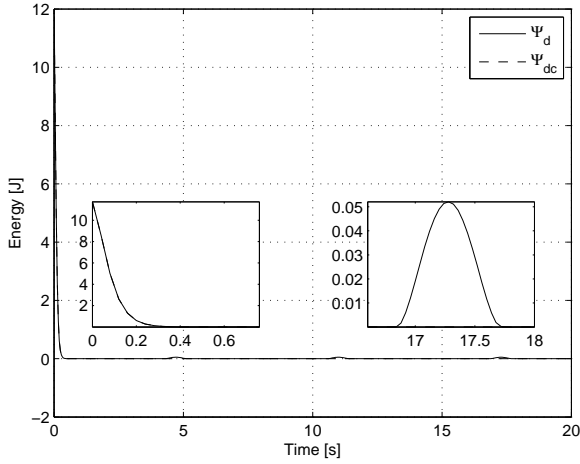


Fig. 8. Navigation error functions - Ψ_d vs Ψ_{dc}

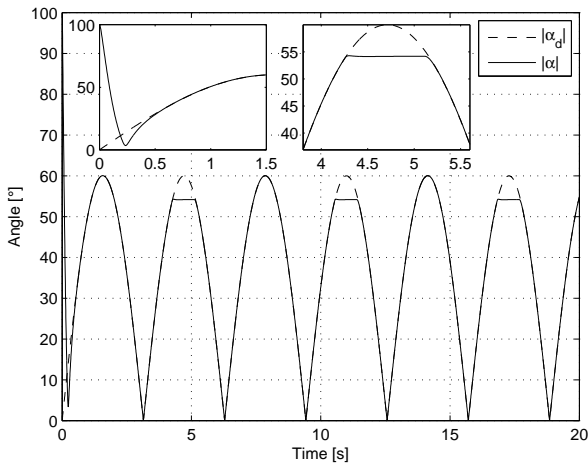


Fig. 9. Angle of inclination - $|\alpha|$ vs $|\alpha_d|$

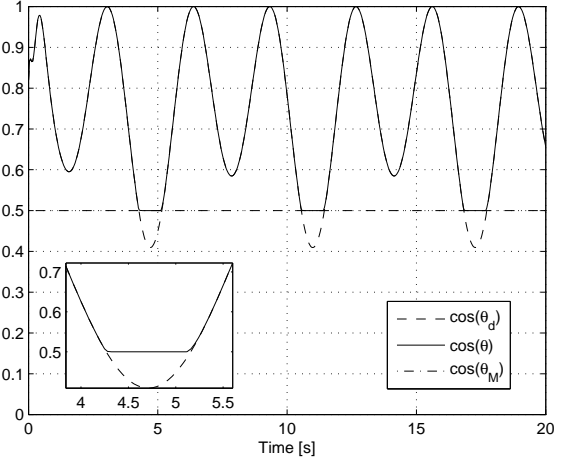


Fig. 10. Cone region validation - $\cos(\theta_d)$ vs $\cos(\theta)$

in a non-linear manifold, and experimental testing of the proposed control law.

References

- [1] S.P. Bhat and D. Bernstein. A topological obstruction to continuous global stabilization of rotational motion and the unwinding phenomenon. *Systems & Control Letters*, 39(1):63–70, 2000.
- [2] F. Bullo and Murray R. M. Tracking for fully actuated mechanical systems: a geometric framework. *Automatica*, 35(1):17–34, jan 1999.
- [3] Z. Cai, M. S. de Queiroz, and D. M. Dawson. A sufficiently smooth projection operator. *IEEE Transactions on Automatic Control*, 51(1):135–139, Jan 2006.
- [4] B. Crowther, A. Lanzon, M. Maya-Gonzalez, and D. Langkamp. Kinematic analysis and control design for a nonplanar multirotor vehicle. *Journal of Guidance, Control, and Dynamics*, 34(4):1157–1171, 2011.
- [5] T. Fernando, J. Chandiramani, T. Lee, and H. Gutierrezee. Robust adaptive geometric tracking controls on $SO(3)$ with an application to the attitude dynamics of a quadrotor UAV. In *50th IEEE Conference on Decision and Control and European Control Conference*, pages 7380–7385, December 2011.
- [6] Formentin, S. and Lovera, M. Flatness-based control of a quadrotor helicopter via feedforward linearization. In *50th IEEE Conference on Decision and Control and European Control Conference, Orlando, USA, 2011*.
- [7] A. Franchi, R. Carli, D. Bicego, and M. Ryll. Full-Pose Geometric Tracking Control on $SE(3)$ for Laterally Bounded Fully-Actuated Aerial Vehicles. *arXiv:1605.06645*, May 2016.
- [8] M.D. Hua, T. Hamel, P. Morin, and C. Samson. Control of VTOL vehicles with thrust-tilting augmentation. *Automatica*, 52:1–7, feb 2015.
- [9] D. Invernizzi and M. Lovera. Geometric tracking control of a quadcopter tiltrotor UAV. In *20th IFAC World Congress, Toulouse, France. Accepted, 2017*.
- [10] G. Jiang and R. Voyles. A nonparallel hexrotor UAV with faster response to disturbances for precision position keeping. In *2014 IEEE International Symposium on Safety, Security, and Rescue Robotics*, pages 1–5. IEEE, 2014.

- [11] D. Kastelan, M. Konz, and J. Rudolph. Fully actuated tricopter with pilot-supporting control. *IFAC-PapersOnLine*, 48(9):79–84, 2015.
- [12] E. Kaufman, K. Caldwell, D. Lee, and T. Lee. Design and development of a free-floating hexrotor UAV for 6-dof maneuvers. In *2014 IEEE Aerospace Conference*, pages 1–10. IEEE, 2014.
- [13] E. Lavretsky and K. A. Wise. Robust and adaptive control: With aerospace applications. *Advanced textbooks in control and signal processing*. London and New York: Springer, 2013.
- [14] T. Lee, M. Leok, and H. McClamroch. Geometric tracking control of a quadrotor UAV on SE(3). In *IEEE Conference on Decision and Control, Atlanta, USA, 2010*.
- [15] Y. Long, L. Wang, and D. J. Cappelleri. Modeling and global trajectory tracking control for an over-actuated MAV. *Advanced Robotics*, 28(3):145–155, 2014.
- [16] C. Micheli, M. Giurato, and M. Lovera. Design, identification and control of a tiltrotor quadcopter UAV. *Submitted*, 2017.
- [17] R. Naldi, M. Furci, R. G. Sanfelice, and L. Marconi. Robust global trajectory tracking for underactuated vtol aerial vehicles using inner-outer loop control paradigms. *IEEE Transactions on Automatic Control*, 62(1):97–112, 2017.
- [18] A. Oosedo, S. Abiko, S. Narasaki, A. Kuno, A. Konno, and M. Uchiyama. Flight control systems of a quad tilt rotor unmanned aerial vehicle for a large attitude change. In *2015 IEEE International Conference on Robotics and Automation*, pages 2326–2331. IEEE, 2015.
- [19] S. Rajappa, M. Ryll, H. H. Bühlhoff, and A. Franchi. Modeling, control and design optimization for a fully-actuated hexarotor aerial vehicle with tilted propellers. In *2015 IEEE International Conference on Robotics and Automation*, pages 4006–4013. IEEE, 2015.
- [20] M. Ryll, H. H. Bühlhoff, and P. Robuffo Giordano. A novel overactuated quadrotor unmanned aerial vehicle: Modeling, control, and experimental validation. *IEEE Transactions on Control Systems Technology*, 23(2):540–556, March 2015.

A Appendix

A.1 Proof of Proposition 3

A.1.1 Boundedness of the attitude error

The Lyapunov candidate for the rotational motion

$$V_R = \frac{1}{2} e_\omega^T I e_\omega + \Psi(R_e) \quad (\text{A.1})$$

is locally positive definite and quadratic for $\Psi < \psi$. Taking the time derivative along the error trajectories one gets

$$\begin{aligned} \dot{V}_R &= \langle d_{R_e} V_R, \dot{R}_e \rangle + \langle d_{e_\omega} V_R, \dot{e}_\omega \rangle \\ &= e_\omega^T I \dot{e}_\omega + e_\omega^T R_d^T (T_I L_{R_e}^* d_{R_e} \Psi) = -e_\omega^T K_\omega e_\omega \leq 0. \end{aligned} \quad (\text{A.2})$$

Thus, the Lyapunov candidate is non-increasing and the navigation function Ψ is bounded by $\Psi \leq V_R(t) \leq V_R(0)$. Selecting the initial conditions such that

$$\frac{1}{2} e_\omega^T(0) I e_\omega(0) + \Psi(R_e(0)) < \psi, \quad (\text{A.3})$$

the attitude error $R_e(t)$ is always inside the set

$$\mathbb{D}_R = \{R \in \text{SO}(3) : \Psi(R) < \psi\}. \quad (\text{A.4})$$

A.1.2 Exponential stability

Consider now the modified Lyapunov candidate,

$$V_R = \frac{1}{2} e_\omega^T I e_\omega + \Psi(R_e) + p_1 e_\omega^T e_R \quad (\text{A.5})$$

for a positive constant p_1 . Letting now $z_R = \{\|e_R\|, \|e_\omega\|\}^T$ one has that

$$\lambda_m(P_{R1}) \|z_R\|^2 \leq V_R \leq \lambda_M(P_{R2}) \|z_R\|^2, \quad (\text{A.6})$$

where

$$P_{R1} = \begin{bmatrix} h_1 & -p_1 \\ -p_1 & \lambda_m(I) \end{bmatrix} \quad P_{R2} = \begin{bmatrix} h_2 & p_1 \\ p_1 & \lambda_M(I) \end{bmatrix}, \quad (\text{A.7})$$

provided that $p_1 < \sqrt{h_1 \lambda_m(I)}$. The time derivative

$$\begin{aligned} \dot{V}_R &= \langle d_{e_\omega} V, \dot{e}_\omega \rangle + \langle d_{R_e} V, \dot{R}_e \rangle \\ &= e_\omega^T I \dot{e}_\omega + e_\omega^T R_d^T e_R + p_1 \dot{e}_R^T e_\omega + p_1 e_R^T \dot{e}_\omega \\ &= -e_\omega^T K_\omega e_\omega + p_1 E(R_e, R_d) e_\omega^T e_\omega \\ &\quad - p_1 e_R^T I^{-1} (R_d^T e_R + K_\omega e_\omega) \end{aligned} \quad (\text{A.8})$$

is bounded by

$$\begin{aligned} \dot{V}_R &\leq -\lambda_m(K_\omega) \|e_\omega\|^2 + p_1 \|E(R_e, R_d)\| \|e_\omega\|^2 \\ &\quad - \frac{p_1}{\lambda_M(I)} \|e_R\|^2 + p_1 \frac{\lambda_M(K_\omega)}{\lambda_m(I)} \|e_\omega\| \|e_R\| \\ &\leq -\lambda_m(W_R) \|z_R\|^2 \end{aligned} \quad (\text{A.9})$$

where

$$W_R = \begin{bmatrix} \frac{p_1}{\lambda_M(I)} & -\frac{p_1}{2} \frac{\lambda_M(K_\omega)}{\lambda_m(I)} \\ -\frac{p_1}{2} \frac{\lambda_M(K_\omega)}{\lambda_m(I)} & \lambda_m(K_\omega) - p_1 \frac{1}{\sqrt{2}} \text{tr}(K_R) \end{bmatrix}. \quad (\text{A.10})$$

Hence, for positive definite matrices K_R and K_ω , by selecting a constant p_1 such that

$$p_1 < \min \left\{ \sqrt{h_1 \lambda_m(I)}, \frac{4\sqrt{2} \lambda_m(K_\omega) \lambda_m(I)^2}{\sqrt{2} \lambda_M(K_\omega)^2 \lambda_M(I) + 4 \text{tr}(K_R) \lambda_m(I)^2} \right\} \quad (\text{A.11})$$

the exponential convergence of the attitude motion can be stated, when the initial condition are inside the domain given by (A.3).

A.2 Proof of Proposition 5

A.2.1 Translational motion analysis

Consider the following modified Lyapunov candidate for the translational motion:

$$V_x(e_x, e_v) = \frac{1}{2}m e_v^T e_v + \frac{1}{2}e_x^T K_x e_x + p_2 e_x^T e_v \quad (\text{A.12})$$

which is positive definite, defining $z_x = \{\|e_x\|, \|e_v\|\}^T$

$$\lambda_m(P_{x1}) \|z_x\|^2 \leq V_x \leq \lambda_M(P_{x2}) \|z_x\|^2 \quad (\text{A.13})$$

$$P_{x1} = \begin{bmatrix} \lambda_m(K_x) & -p_2 \\ -p_2 & m \end{bmatrix} \quad P_{x2} = \begin{bmatrix} \lambda_M(K_x) & p_2 \\ p_2 & m \end{bmatrix}, \quad (\text{A.14})$$

provided that $p_2 < \sqrt{m\lambda_m(K_x)}$. The time derivative of V_x reads

$$\begin{aligned} \dot{V}_x &= \langle d_{e_v} V, \dot{e}_v \rangle + \langle d_{e_x} V, \dot{e}_x \rangle \\ &= m e_v^T \dot{e}_v + c_1 e_x^T \dot{e}_v + e_v^T K_x e_x + c_1 e_v^T e_v \\ &= e_v^T (-m g e_3 + f_c^d - f_c^d + R f_c - m \dot{v}_d + K_x e_x + p_2 e_v) \\ &\quad + \frac{p_2}{m} e_x^T (-m g e_3 + f_c^d - f_c^d + R f_c - m \dot{v}_d) \\ &= -e_v^T (K_v e_v - (R f_c - f_c^d) - p_2 e_v) + \frac{p_2}{m} e_x^T (-K_v e_v \\ &\quad - K_x e_x + (R f_c - f_c^d)) = -e_v^T (K_v - p_2 I_{3 \times 3}) e_v \\ &\quad - \frac{p_2}{m} e_x^T K_x e_x - \frac{p_2}{m} e_x^T K_v e_v + \left(\frac{p_2}{m} e_x^T + e_v^T \right) \Delta f_c, \end{aligned} \quad (\text{A.15})$$

where the vector $\Delta f_c = R f_c - f_c^d$ represents the difference between the desired control force and the actual one:

$$\Delta f_c = R c(\Psi) R_d^T f_c^d - f_c^d = (c(\Psi) R_e - I_{3 \times 3}) f_c^d. \quad (\text{A.16})$$

By exploiting the following inequality (which follows from equation (31))

$$\Psi \geq \frac{1}{2} \lambda_m(K_R) \text{tr}(I_{3 \times 3} - R_e) \rightarrow \text{tr}(R_e) \geq 3 - \frac{2\Psi}{\lambda_m(K_R)}$$

the norm of the vector Δf_c is bounded by:

$$\begin{aligned} \|\Delta f_c\| &\leq \|c(\Psi) R_e - I_{3 \times 3}\| \|f_c^d\| \\ &\leq \|c(\Psi) R_e - I_{3 \times 3}\|_F \|f_c^d\| \\ &= \sqrt{\text{tr} \left((c(\Psi) R_e - I_{3 \times 3})^T (c(\Psi) R_e - I_{3 \times 3}) \right)} \|f_c^d\| \\ &= \sqrt{\text{tr} \left(c(\Psi)^2 I_{3 \times 3} - c(\Psi) (R_e + R_e^T) + I_{3 \times 3} \right)} \|f_c^d\| \\ &= \sqrt{3 \left(1 + c(\Psi)^2 \right) - c(\Psi) \text{tr}(R_e + R_e^T)} \|f_c^d\| \\ &= \sqrt{3 \left(1 + c(\Psi)^2 \right) - 2c(\Psi) \text{tr}(R_e)} \|f_c^d\| \\ &\leq \sqrt{3 \left(1 + c(\Psi)^2 \right) - 2c(\Psi) \left(3 - \frac{2\Psi}{\lambda_m(K_R)} \right)} \|f_c^d\| \\ &= \sqrt{3 + 3 \left(1 - \frac{\Psi}{\Psi_M} \right)^2 - \left(2 - \frac{2\Psi}{\Psi_M} \right) \left(3 - \gamma \frac{\Psi}{\Psi_M} \right)} \|f_c^d\| \\ &= \sqrt{\left((3 - 2\gamma) \left(\frac{\Psi}{\Psi_M} \right)^2 + 2\gamma \frac{\Psi}{\Psi_M} \right)} \|f_c^d\| \\ &\leq \sqrt{(3 + 2\gamma) \frac{h_2}{\Psi_M}} \|e_R\| \|f_c^d\| = \alpha \|e_R\| \|f_c^d\| \quad (\text{A.17}) \end{aligned}$$

where $\gamma = \frac{2}{\lambda_m(K_R)}$ and $\alpha = \sqrt{(3 + 2\gamma) \frac{h_2}{\Psi_M}}$. Finally, the time derivative of V_x is bounded by

$$\begin{aligned} \dot{V}_x &\leq -(\lambda_m(K_v) - p_2) \|e_v\|^2 - \frac{p_2}{m} \lambda_m(K_x) \|e_x\|^2 \\ &\quad + \frac{p_2}{m} \lambda_M(K_v) \|e_x\| \|e_v\| + \alpha f_M \left(\frac{p_2}{m} \|e_x\| + \|e_v\| \right) \|e_R\| \end{aligned} \quad (\text{A.18})$$

where it is assumed that $\|K_x e_x + K_v e_v\| \leq f_{cM}$ so that $\|f_c^d\| \leq f_{cM} + f_M^d \leq f_M$, $f_M^d = \sup_{t \geq t_0} (\|m g e_3 + m \dot{v}_d\|)$.

Hence, the Lyapunov analysis is conducted in the set $\{\{e_x, e_v\} \in \mathbb{R}^3 \times \mathbb{R}^3 : \|K_x e_x + K_v e_v\| \leq f_{cM}\}$.

A.2.2 Full motion

Since the translational motion depends on the attitude error through the control force, a Lyapunov candidate for the complete system must be defined:

$$V(R_e, e_x, e_\omega, e_v) = V_x + V_R \quad (\text{A.19})$$

which is positive definite and quadratic

$$\lambda_m(P_1) \|z\|^2 \leq V \leq \lambda_M(P_2) \|z\|^2 \quad (\text{A.20})$$

$$P_1 = \begin{bmatrix} P_{x1} & 0 \\ 0 & P_{R1} \end{bmatrix} \quad P_2 = \begin{bmatrix} P_{x2} & 0 \\ 0 & P_{R2} \end{bmatrix} \quad (\text{A.21})$$

for $\Psi < \psi$ provided that $p_1 < \sqrt{h_1 \lambda_m(I)}$ and $p_2 < \sqrt{m \lambda_m(K_x)}$.

Combining the results of (A.9) and (A.18) we get:

$$\begin{aligned} \dot{V} \leq & -\lambda_m(W_x) \|z_x\|^2 - \lambda_m(W_R) \|z_R\|^2 \\ & + \|W_{Rx}\|_2 \|z_x\| \|z_R\| \leq -\lambda_m(W) \|z\|^2 \end{aligned} \quad (\text{A.22})$$

where

$$\begin{aligned} W_x &= \begin{bmatrix} \frac{p_2}{m} \lambda_m(K_x) & -\frac{p_2}{2m} \lambda_M(K_v) \\ -\frac{p_2}{2m} \lambda_M(K_v) & \lambda_m(K_v) - p_2 \end{bmatrix} \\ W_{Rx} &= \begin{bmatrix} \frac{p_2}{m} \alpha f_M & 0 \\ \alpha f_M & 0 \end{bmatrix} \quad W = \begin{bmatrix} \lambda_m(W_x) & -\frac{\|W_{Rx}\|_2}{2} \\ -\frac{\|W_{Rx}\|_2}{2} & \lambda_m(W_R) \end{bmatrix}. \end{aligned} \quad (\text{A.23})$$

For positive constants $\lambda_m(K_x)$, $\lambda_m(K_v)$, $\lambda_M(K_v)$ the remaining parameters p_1 , p_2 , $\lambda_m(K_\omega)$, $\lambda_M(K_\omega)$ and k_{R_1} , k_{R_2} , k_{R_3} are selected such that

$$p_1 < \min \left\{ \sqrt{h_1 \lambda_m(I)}, \frac{4\sqrt{2} \lambda_m(K_\omega) \lambda_m(I)^2}{\sqrt{2} \lambda_M(K_\omega)^2 \lambda_M(I) + 4tr(K_R) \lambda_m(I)^2} \right\} \quad (\text{A.24})$$

$$p_2 < \min \left\{ \sqrt{m \lambda_m(K_x)}, \frac{4m \lambda_m(K_v) \lambda_m(K_x)}{4m \lambda_m(K_x) + \lambda_M(K_v)^2} \right\} \quad (\text{A.25})$$

$$\lambda_m(W_x) > \frac{\|W_{Rx}\|_2^2}{4\lambda_m(W_R)}. \quad (\text{A.26})$$

Correspondingly, there exist positive definite matrices K_x , K_v , K_ω and $K_R = \text{diag}(k_{R_1}, k_{R_2}, k_{R_3})$. Then, the zero equilibrium of the closed-loop tracking errors $(e_x, e_R, e_v, e_\omega)$ is exponentially stable.

Finally, to show the bound (52), consider the following inequalities:

$$\|K_x e_x + K_v e_v\| \quad (\text{A.27})$$

$$\leq \max \left(\sqrt{\lambda_M(K_x^T K_x)}, \sqrt{\lambda_M(K_v^T K_v)} \right) (\|e_x\| + \|e_v\|)$$

$$\|e_x\| + \|e_v\| \leq \sqrt{2} \sqrt{(\|e_x\|^2 + \|e_v\|^2)} \quad (\text{A.28})$$

from which one gets

$$\|K_x e_x + K_v e_v\| \quad (\text{A.29})$$

$$\leq \sqrt{2} \max \left(\sqrt{\lambda_M(K_x^T K_x)}, \sqrt{\lambda_M(K_v^T K_v)} \right) \|z_x\|.$$

Then, equation (52) follows by combining (A.29),

$$\lambda_m(P_{x1}) \|z_x\|^2 \leq V_x \leq V_x + V_R = V \quad (\text{A.30})$$

$$\rightarrow \|z_x\| \leq \sqrt{\frac{V(0)}{\lambda_m(P_{x1})}} \quad (\text{A.31})$$

and the requirement that $\|K_x e_x + K_v e_v\| < f_{c_M}$.